Current and ultimate limitations of scanning x-ray nanotomography

I. McNulty
Advanced Photon Source, Argonne National Laboratory, 9700 S. Cass Avenue, Argonne, IL 60439 USA

ABSTRACT

X-ray nanotomography has developed into a powerful new tool for three-dimensional structural analysis. The scanning approach offers capabilities that are competitive with full-field imaging. Current and ultimate limitations of nanotomography are examined in light of recent work.

Keywords: scanning x-ray microscope, 3D imaging, nanotomography, tomography, nano-scale

1. INTRODUCTION

Three-dimensional (3D) tomographic microscopy has been developed and applied to a variety of biological and materials science problems at a resolution well below the 1 μm scale using soft [1-4] and intermediate energy x-rays [5,6]. In these experiments, a series of two-dimensional (2D) projection images is acquired over a wide angular range through the sample, either by recording the pixels serially (scanning microscope) or by imaging all the pixels at once (full-field microscope). The state of the art in 3D imaging resolution is currently shared by both types of x-ray microscopes. On the one hand, full-field imaging offers a substantial speed advantage, as all pixels in each tomographic projection are acquired in parallel, and straightforward adaptation to phase-contrast imaging. Holographic tomography [7] also benefits from parallel acquisition and offers phase sensitivity but requires more complex reconstruction algorithms.

On the other hand, the slower scanning approach offers quantitative data acquisition, a larger field of view without field stitching, and less dose delivered to the sample. Quantitation over a large detective dynamic range is facilitated using photon-counting detection and computer-controlled acquisition. The scanned view-field can, in principle, be as large as the scan range and is not limited to the objective lens aperture as in the full-field case. Because the x-ray optics precede rather than follow the sample, best use can also made of the radiation transmitted by the sample, therefore less dose is deposited than in the full-field case, where an objective lens transports the object image to the detector.

Currently, there are several scanning transmission x-ray microscopes (STXMs) with ~100 nm resolution or better operating at the National Synchrotron Light Source, Advanced Photon Source, and Advanced Light Source [8-11]. Instruments at the first two facilities have been used for nanotomography. Others under development have proposed nanotomography programs in both the soft and intermediate x-ray regions [12,13], and scanning tomography is being developed with a hard x-ray microscope at 300 nm resolution [14]. These instruments use x-ray photoabsorption as the image contrast mechanism. Fluorescence tomography by scanning, albeit at lower resolution, has undergone rapid development in the last few years and offers 3D elemental analysis capability at unprecedented sensitivity [15-17]. Also being explored is use of scanning transmission electron microscopes (STEMs) for nanotomography. STEMs offer fast scan rates and competitive imaging resolution in thin samples. This paper examines the current and ultimate limitations of the scanning approach to transmission x-ray nanotomography in light of recent technical progress.

2. CURRENT METHODS AND LIMITATIONS

2.1 Typical configuration

A typical STXM configuration is shown pictorially in Fig. 1. A high brilliance undulator supplies the instrument with coherent x-ray illumination. A high resolution optic, such as a Fresnel zone plate (ZP), focuses the x-ray beam to a diffraction-limited spot; a pinhole serving as an order-sorting aperture selects the first-order focus and excludes unwanted ZP diffraction orders. The sample is scanned through the focus on a high resolution scan stage under computer control as the transmitted x-ray photons are detected with a photon-counting system, such as an avalanche photodiode or scintillator coupled to a photomultiplier. The detector output pulses are counted by a scaler, also under computer control. Projections through the sample are recorded sequentially as a function of sample orientation to the incident beam.

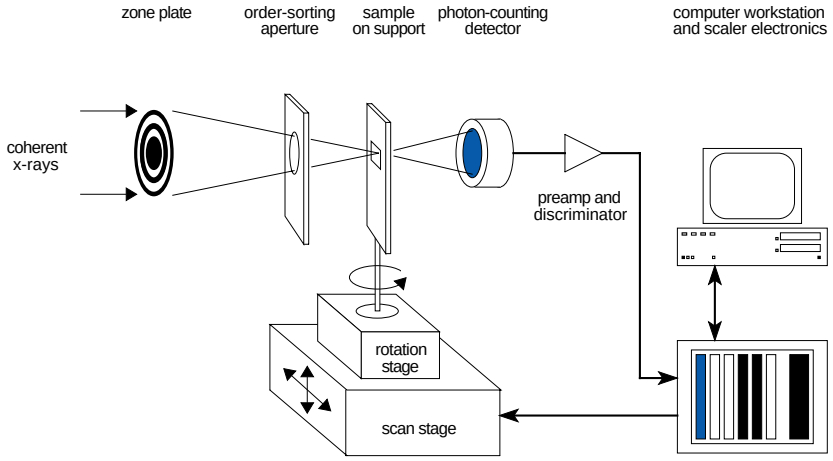

Fig. 1. Typical scanning transmission x-ray microscope configuration.

2.2 Sample stage

STXMs traditionally achieve both large range and high scan resolution by using a combination of coarse and fine resolution xy positioners to scan the sample. The coarse stage is driven by stepper or DC motors, has a much lower resolution (0.1-1 μm) than the fine scan stage, and much larger range (many mm) for large alignment scans and sample insertion and retraction. The fine scan stage (fig. 2) typically has two flexure-type translation axes driven by piezoelectric actuators with a resolution of ~1 nm and range of ~100 μm. Integral position feedback, either by capacitance or strain-gauge micrometry, is now standard. The sample is oriented for each tomographic projection on a precision rotation stage, either mounted atop or beneath the linear scan stage assembly. If mounted on the fine scan stage, the rotation stage must have low mass and high stiffness in order not to degrade the quality of the scan motion.

The capability to perform scans "on-the-fly" is now commonplace, in which the timing of the pixels in each scan line is handled in hardware. By contrast to the "step-and-repeat" scan method, the on-the-fly approach only incurs software overhead at the start of each scan line rather than once per pixel, enabling continuous scanning as fast as the stage assembly and photon statistics permit. Motor-driven mechanical stages are limited to maximum velocities of a few mm/s. Piezoelectric stages are much lighter, faster, and stiffer, with peak velocities usually limited by the driving electronics to 10-20 mm/s and lowest-mode resonances of 200-500 Hz. Greater speeds are possible due to the inherent stiffness of piezoelectric stages, but

at the cost of more complex, fast-risetime electronics. A recent development is the availability of tuned control using digital signal processing methods to achieve higher positioning performance, for instance, by overdamping.

(a) (b)

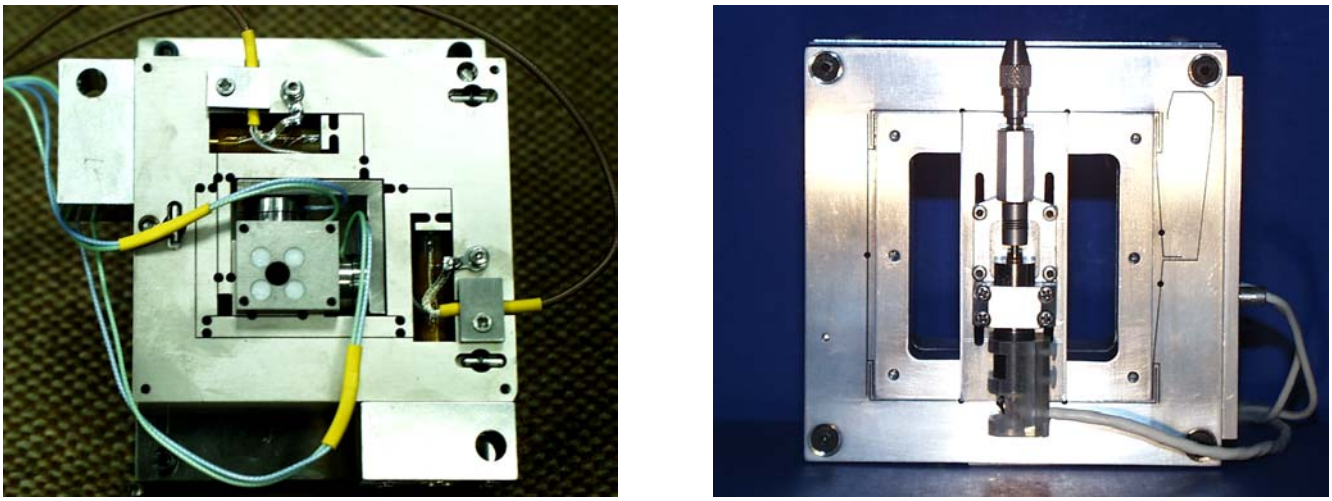

Fig. 2. Two types of fine scan stages. (a) Older design with composite xy flexure stage using capacitance micrometry, by Queensgate Instruments, Inc. (b) Newer design with separate x and y stages using strain-gauge micrometry, by Mad City Labs, Inc. Precision stepper-motor rotation stage is shown mounted on xy stage assembly.

2.3 Scan errors

Imaging defects arising from scan errors and other position changes between the nanofocus and sample currently pose the greatest obstacles confronting precision scanning nanotomography. These can take several forms depending upon the origin and time scale of the errors and may or may not be correctable *a posteriori* (table 1). Correcting projection data for scan stage jitter and irreproducibility due to vibration and noise (fast time scales) or drift (slow time scales) is difficult without some *a priori* knowledge of the sample and otherwise impossible due to the unpredictability of these errors (figs. 3,4). Similarly, compliance in the rotation stage or sample mount can lead to uncorrectable scan errors due to inertial effects. By contrast, deterministic scan errors, such as field curvature, axis nonorthogonality, and axis scale mismatch, are comparatively easy to correct. In order for an error to be correctable, it must either be static or drift predictably in time. Nanotomographic 3D imaging is far more sensitive to scan errors than simple 2D imaging, because accurate 3D reconstruction depends on geometrical stability throughout the entire project set. Repeating scans to mitigate errors increases the total time and radiation dose; this has been a factor in work to date, limiting collection of more than ~20 projections in a set [1,3,5,6]. Considerable effort has therefore been spent on bringing STXM performance to the level where these errors are negligible or infrequent.

Table 1. Types of scan stage errors, associated time scales, and post-acquisition correctability. The relative time scales "fast" and "slow" are defined as occurring on a per-pixel basis and a per-line basis, respectively.

Scan error type	Time scale	Correctable
position jitter	fast	no
position irreproducibility	fast	no
position drift	slow	yes
field curvature	slow	yes
axis nonorthogonality	slow	yes

axis scale mismatch	slow	yes

(a) (b)

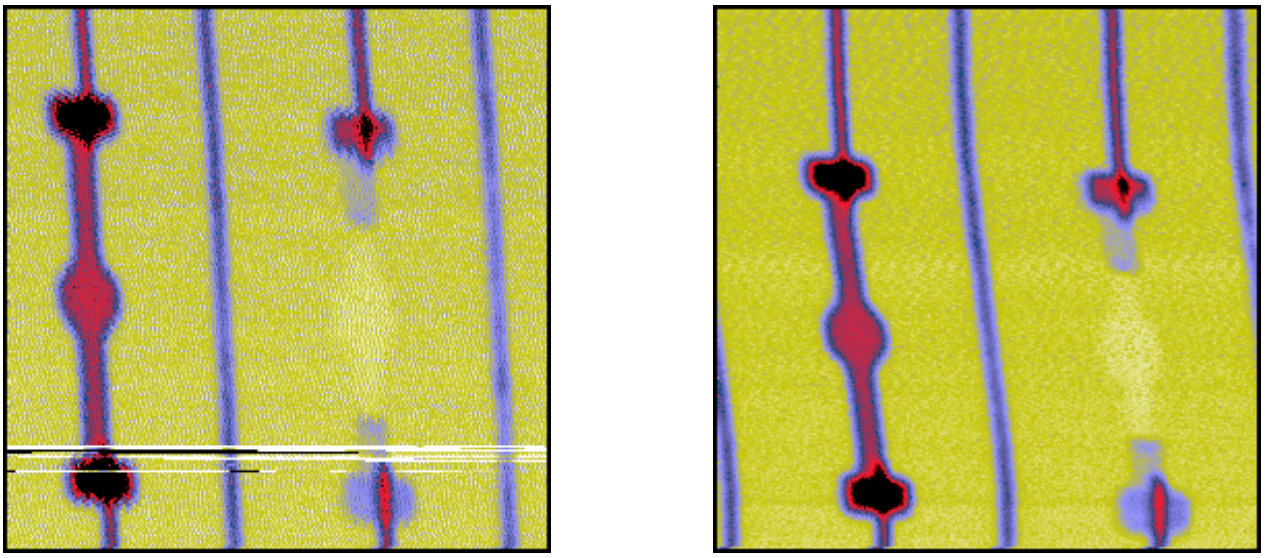

Fig. 3. Examples of scan errors. (a) Scan of 5 µm x 5 µm area in a Cu/Si test pattern containing two interconnects (one intact, one failed). The scan geometry has few errors, although several scan lines are defective. (b) Poor quality scan showing severe geometric distortion due to drift during the scan.

(a) (b)

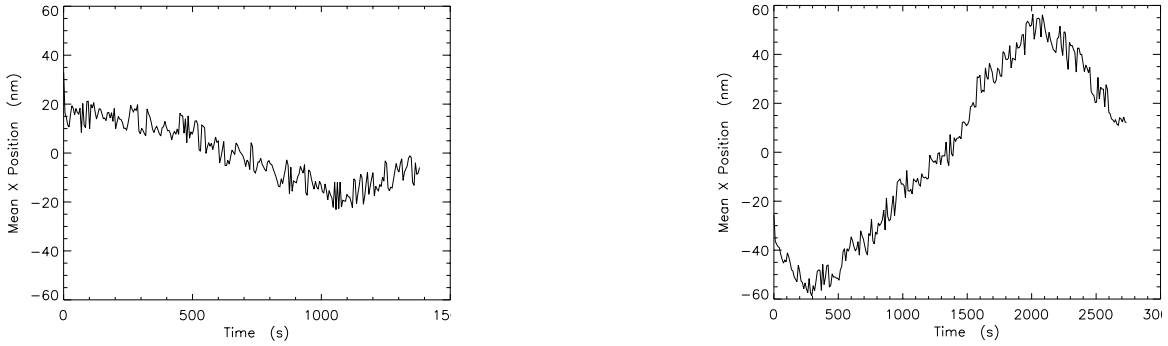

Fig. 4. Mean position of the sample stage along the x (horizontal) axis as a function of time during scans in fig. 3. (a) X-axis drift was no more than ±20 nm in fig. 3a, whereas (b) it was nearly ±60 nm in fig. 3b, causing obvious distortion. The drift was probably due to cycling of the room air conditioning system governing the stage temperature.

Fixed geometrical distortions have been corrected using first-order polynomial warping [10] and least-squares methods [6,18] to fit the data to the known dimensions of a test object. These approaches are successful in correcting the principal distortions in 2D scan data, even where the relative angle between the scan axes is as large as 15°, which has been observed in stages with significant xy coupling [10]. Once calibrated, the correction coefficients can also be used to drive the stage in a properly scaled, orthogonal manner. However in nanotomography applications, the calibration effort required to achieve

fully corrected scan motion over a wide angular range of the sample becomes prodigious, as the problem has up to six degrees of freedom.

2.4 Sample targeting

An essential consideration for scanning nanotomography is the accuracy with which the nanofocus can be targeted onto the sample region of interest (ROI) over a large angular range. Precise pre-alignment of the ROI to the rotation axis of the sample rotation stage greatly reduces the need for post-acquisition alignment of the projections. This is limited by the radial and angular runout of the rotation stage. Some efforts (only at the micrometer resolution scale to date) have focused on using low-runout air-bearing rotation stages, which unfortunately are too bulky at present for scanning nanotomography. In addition, the depth of field for ZPs used in nanofocus STXMs is as short as a few micrometers, comparable to the precision with which the ROI can be centered on the sample rotation axis and to the runout of the best stages used to focus the beam onto the sample. Sample targeting again becomes a six-axis problem when the eccentricities in the ROI rotation exceed the depth of field, due to focusing stage runout.

One way around ROI position uncertainties relative to the nanofocus is to scan the sample over a larger range in x, y, and θ than that needed to reconstruct the ROI, allowing for the largest uncertainty. The projections are then aligned to one another by cross-correlation or other means, in analogy to x,y,energy "stack" methods [19]. Another is to map the interdependence of the x,y,θ stage coordinates for the ROI in advance of the data acquisition, assuming the uncertainties are sufficiently reproducible. Straightforward application of the polar relationship

$$x = x_0 + R\cos(\theta + \theta_0), \quad z = z_0 + R\sin(\theta + \theta_0)$$

has worked well in experiments with the 2-ID-B STXM at the Advanced Photon Source [6], where the rotation angle θ is about the y-axis, R is the radius of rotation, and x_0, z_0, and θ_0 are the initial ROI position and angular offsets. The radius can be quickly determined from two projections spaced 180° apart, and the offsets found using two more projections at 90° intervals. Nonperpendicularity between the various motion axes (xy, xz, yz) also results in θ-dependent targeting error, posing a limit to this method. Nevertheless, this method has the advantage of making it possible to obtain all the projection data quickly and consecutively, minimizing signal drift and systematic position errors, at the cost of the time required to "pre-map" the scan uncertainties as a function of θ. It also facilitates automated acquisition of all the projections. In practice, a combination of both pre-alignment and overscanning are used.

3. ULTIMATE LIMITS

3.1 Inertial limits

The high resonant frequencies of piezoelectric stages in current use permit stage velocities that currently exceed the capabilities of most electronics systems available to drive them. Provided such electronics become available, the peak velocity that could be achieved with a stage having a lowest resonant frequency f_0 and range x_{max} is $v_{max} = f_0 x_{max}$. The minimum pixel dwell time $t_{min} = 1/(f_0 N)$ also follows from the resonant frequency, where N is the number of pixels per scan line. Consequently, the maximum acceleration experienced by the sample on the stage, assuming the peak velocity is reached within the first pixel, is $a_{max} = v_{max}/t_{min}$. With f_0 = 500 Hz, x_{max} = 100 μm, and N = 1000, v_{max} = 50 mm/s and $a_{max} = 2.5 \times 10^4$ m/s^2 ~ 2.5 x 10^3 G's ! Clearly, this extreme acceleration at the endpoints of a fast scan will be hard on the sample and may permanently alter its morphology, if not dislodge it from its support (table cloth and silverware effect). Even if sample damage does not occur, unwanted motion due to inertial effects will likely limit the imaging resolution, depending on the rigidity of both the optics and the mounted sample. By contrast, STEMs are not subject to this limitation because the electron probe beam is scanned rather than the sample.

3.2 Source brilliance and photon statistics

Scanning x-ray micoscopes using undulator sources with a brilliance of 10^{18} - 10^{19} ph/mm^2/mrad^2/s/0.1% BW, beamlines with efficiencies of 5-10% (soft x-rays) or 80-90% (hard x-rays), and ZPs with diffraction efficiencies of 10-20% are typical

of instruments at third-generation synchrotron storage rings. Consequently, a spectral flux of 10^7 - 10^9 ph/s/0.1% BW is routinely obtained at the nanofocus of these instruments. Ignoring additional noise arising from the source, stability of the optics, and detector, one could dwell as short as 100 μs/pixel with this focused flux and still obtain 1% Poisson-limited statistics in each scan pixel. This corresponds to a peak velocity of $v_{max} = x_{max}/(Nt_{min}) = 1$ mm/s for the scan parameters given above, much less than that for the scan stage alone. Another order-of-magnitude increase in source brilliance will shift the ultimate limitation from photon statistics to the scan stage speed and sample rigidity. As the brilliance of next-generation x-ray sources increases, we can expect it to outpace the limits of mechanical scan systems.

ACKNOWLEDGMENTS

The author gratefully acknowledges S. Frigo, Y. Wang, C. Retsch, and J. Arko for their dedication bringing the 2-ID-B STXM to fruition, Z. Levine, S. Grantham, T. Lucatorto, and C. Tarrio for much experimental help and useful discussion, and I. Noyan of IBM Corp. for providing the test object in fig. 3. This work is supported by the U.S. Department of Energy, Basic Energy Sciences, Office of Science, under contract W-31-109-ENG-38.

REFERENCES

1. W.S. Haddad, et al., *Science* **266**, 1213 (1994).
2. J. Lehr, et al., *Optik* **104**, 166 (1997).
3. Y. Wang, C. Jacobsen, J. Maser, and A. Osanna, *J. Microscopy* **197**, 80 (2000).
4. D. Weiß, et al., *Ultramicroscopy* **84**, 185 (2000).
5. Z.H. Levine, A.R. Kalukin, S.P. Frigo, I. McNulty, and M. Kuhn, *Appl. Phys. Lett.* **74**, 150 (1999).
6. Z.H. Levine, et al., *J. Appl. Phys*. **87**, 4483 (2000).
7. P. Cloetens, et al., *Appl. Phys. Lett.* **75**, 2912 (1999).
8. C. Jacobsen et al., *Opt. Commun.* **86**, 351 (1991).
9. I. McNulty, W.S. Haddad, J.E. Trebes, and E.H. Anderson, *Rev. Sci. Instrum.* **66**, 1431 (1995).
10. I. McNulty, et al., *SPIE Proc.* **3449**, 67 (1998).
11. T. Warwick, et al., *Rev. Sci. Instrum.* **69**, 2964 (1998).
12. P. Guttman, et al., *Am. Inst. Phys.* **CP507**, 411 (2000).
13. J. Susini, R. Barrett, B. Kaulich, S. Oestreich, and M. Salomé, *Am. Inst. Phys.* **CP507**, 19 (2000).
14. Z. Cai, et al., *Am. Inst. Phys.* **CP521**, 31 (2000).
15. M. Naghedolfeizi, J.-S. Chung, G.E. Ice, W. Yun, Z. Cai, and B. Lai, *Mat. Res. Soc. Symp. Proc.* **524**, 233 (1998).
16. S.R. Sutton, G. Flynn, M. Rivers, M. Newville, and P. Eng, *Lunar Planet. Sci.* **31**, 1857 (2000).
17. C. Schroer, et al., *SPIE Proc.* **4503**, in press.
18. A.R. Kalukin, et al., *SPIE Proc.* **3772**, 237 (1999).
19. C. Jacobsen, S. Wirick, G. Flynn, and C. Zimba, *J. Microscopy* **197**, 173 (2000).